Springer

KSME

Journal of Mechanical Science and Technology 25 (1) (2011) 239~246
www.springerlink.com/content/1738-494x
DOI 10.1007/s12206-010-1103-z

Driving an AMB system using a 2D space vector modulation of three-leg voltage source converters †

Hyeong-Joon Ahn[1,*] and Se-Na Jeong[2]

[1]*Department of Mechanical Engineering, Soongsil University, 511 Sangdo-dong, Dongjak-gu, Seoul 156-743, Korea*
[2]*Graduate School, Department of Mechanical Engineering, Soongsil University, Sangdo-dong, Dongjak-gu, Seoul 156-743, Korea*

(Manuscript Received October 9, 2009; Revised May 18, 2010; Accepted September 20, 2010)

Abstract

This paper presents new methodologies for driving an active magnetic bearing (AMB) system using a two-dimensional (2D) space vector modulation of three-leg voltage source converters. Two types of driving configurations are proposed: full-performance and economy. The economy configuration is proven to be more cost-effective than the conventional driving configurations. For both driving configurations, conversion rules are developed to calculate the three-leg voltage references from two-coil voltage references of an AMB system. In addition, the potential performance limit of the proposed driving configurations is analyzed. Experimental results are presented using a single degree of freedom (DOF) AMB system to verify the analytical results.

Keywords: Active magnetic bearing; Power amplifier; Space vector modulation; Three-leg voltage source converter

1. Introduction

Active magnetic bearing (AMB) systems have many advantages, such as non-contact lubricant-free operation, high rotational speeds, and flexibility in choosing bearing characteristics [1–2]. However, the cost and the reliability of sophisticated control electronics remain the main obstacles to the development of AMB systems. In particular, the cost of power amplifiers comprises a large portion of the whole system.

Proven technologies of the AC drive industry, such as integrated power devices and control architectures, have rarely been applied to AMB systems. Various power modules have been designed to provide a cost-effective solution as a single package [3]. For example, space vector pulse width modulation (PWM) has proven to be one of the most popular and favorable PWM schemes in the past few decades [4, 5].

Thus far, several types of digital power amplifier schemes have been studied for AMB systems. [6-10]. One example is the synchronous three-level PWM power amplifier, which has low current harmonics, even with low switching frequency [6]. New digital control schemes have also been discussed in the literature for low-cost industrial AMB applications [7]. A three-phase converter has been applied to a three-pole radial AMB system; however, it requires complex winding and also suffered from cross-coupling [8]. Power amplifiers using a space vector PWM were introduced to AMB systems in [9, 10]. Their implementation and experimental validation, however, have not yet been reported.

This paper presents new methodologies for driving an AMB system using a 2D space vector modulation of three-leg voltage source converters. Two driving configurations are proposed: full-performance and economy. The conversion rules of AMB coil voltage references into three-phase converter voltage references are developed. Performance limitations of the proposed driving configurations are analyzed both mathematically and numerically. Results of these analyses are verified experimentally with a single degree of freedom (DOF) AMB system.

2. AMB and its power amplifier

An AMB system usually consists of electromagnets, a target, position sensors, power amplifiers, and a position controller. The AMB system is unstable in open-loop status; however, the target can be stably supported by controlling currents of the electromagnets, using measured displacement of the target. An AMB power amplifier converts a weak control signal into a physical quantity, such as current or voltage that produces a magnetic force. The most common power amplifier is a current control with a differential driving mode, as shown in Fig. 1. In this case, the position controller produces the control

† This paper was recommended for publication in revised form by Associate Editor Kyongsu Yi
* Corresponding author. Tel.: +82 2 820 0654, Fax.: +82 2 820 0668
E-mail address: ahj123@ssu.ac.kr

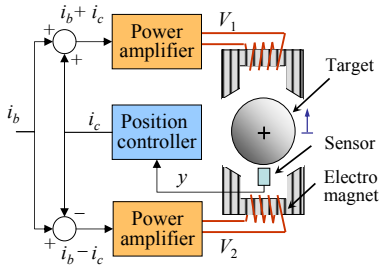

Fig. 1. A single DOF AMB system.

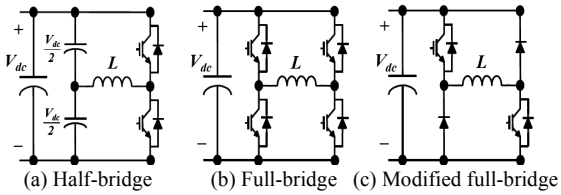

Fig. 2. Driving configurations for AMB systems.

current (i_c) using the measured target displacement (y), and the current controllers produce appropriate voltages (V_1 and V_2) across coils. The AMB system adds a bias current (i_b) to the control current to linearize the current–force relationship and to increase the dynamic stiffness [1].

Fig. 2 shows three typical driving configurations for AMB systems. The most cost-effective scheme among the three driving configurations is the half-bridge scheme in Fig. 2(a). Two DC voltage sources of half amplitude are built up by splitting the DC link voltage ($\pm V_{dc}$) with two capacitors. In this configuration, the balance of the two split DC voltages should carefully be maintained by increasing the capacitor volume or by an active control. The full-bridge scheme uses the whole DC link voltage. This scheme, however, requires twice as many switch elements as the half-bridge scheme, as shown in Fig. 2(b). A cost-effective modified full-bridge scheme is used considering the one-directional current flow of an AMB, as shown in Fig. 2(c).

3. Driving an AMB system using a 2D space vector modulation

3.1 Driving configurations

A two-phase AC motor is composed of two symmetrical windings, which are electrically 90° out of phase. The two-phase motor can be driven using the three-leg voltage source converter shown in Fig. 3. The three-leg voltages of V_a, V_b, and V_c, according to the switching states of S_a, S_b, and S_c, determine the two coil voltages of the motor independently; this is called 2D space vector modulation [11].

The single DOF AMB system shown in Fig. 1 has two coils, similar to a two-phase motor. Therefore a single DOF AMB system can be driven with a three-leg voltage source converter using two different driving configurations (i.e., full-performance and economy), as shown in Fig. 4. In the case of the economy configuration, three of the switching devices and

Table 1. Switching states and coil voltages.

Switching states			Full performance		Economy	
S_a	S_b	S_c	V_1	V_2	V_1	V_2
0	0	0	0	0	$-V_{dc}$	$-V_{dc}$
0	0	1	0	$-V_{dc}$	$-V_{dc}$	0
0	1	0	$-V_{dc}$	$+V_{dc}$	0	0
0	1	1	$-V_{dc}$	0	0	$+V_{dc}$
1	0	0	$+V_{dc}$	0	0	$-V_{dc}$
1	0	1	$+V_{dc}$	$-V_{dc}$	0	0
1	1	0	0	$+V_{dc}$	$+V_{dc}$	0
1	1	1	0	0	$+V_{dc}$	$+V_{dc}$

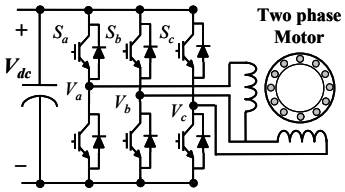

Fig. 3. Driving a two-phase motor with a three-leg voltage source converter.

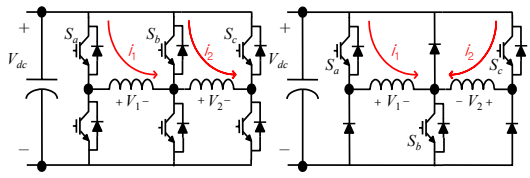

Fig. 4. Driving configurations of an AMB system using a three-leg voltage source converter.

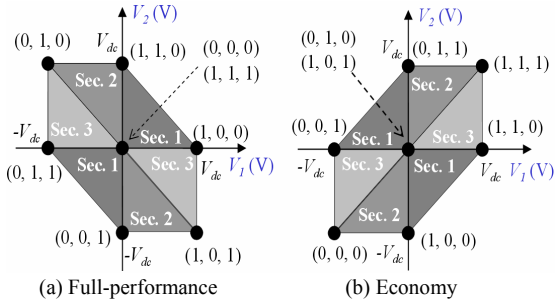

Fig. 5. Available voltage region of two driving configurations.

PWM command outputs can be saved, as well as the energy loss related to the saved switching devices [6]. Therefore, the economy configuration is more cost-effective than other driving configurations (Fig. 2) in terms of material and manufacturing cost.

There are eight switching states in the proposed driving configurations: six active states and two zero states. The coil voltages vary according to the switching states, which are presented in Table 1. There are unavailable voltage pairs: ($\pm V_{dc}$, $\pm V_{dc}$) for the full-performance and ($\pm V_{dc}$, $\mp V_{dc}$) for the economy configurations.

Table 2. Conversion rules of the coil voltage references into the three-leg voltage references.

(a) Full-performance driving configuration

Sec.	a (a+b)>0	ab>0	V_a/ V_{dc}	V_b/ V_{dc}	V_c/ V_{dc}
1	*	T	(1+a+b)/2	(1-a+b)/2	(1-a-b)/2
2	F	F	(1+2a+b)/2	(1+b)/2	(1-b)/2
3	T	F	(1+a)/2	(1-a)/2	(1-a-2b)/2

(b) Economy driving configuration

Sec.	a (a-b)>0	ab>0	V_a/ V_{dc}	V_b/ V_{dc}	V_c/ V_{dc}
1	*	F	(1+a-b)/2	(1-a-b)/2	(1-a+b)/2
2	F	T	(1+2a-b)/2	(1-b)/2	(1+b)/2
3	T	T	(1+a)/2	(1-a)/2	(1-a+2b)/2

A voltage reference vector for the two-coil voltages can be obtained using the 2D space vector modulation. The available voltage regions for two coils of an AMB using 2D space vector modulation are shown in Fig. 5.

Six voltage regions are grouped into three sections, and the combinations of the borderlines of the sections are used as conditions to identify sections from the coil voltage references. For example, a=0, b=0, and a+b=0 are the borderlines of sections in Fig. 5(a), and the combinations of a(a+b)>0 and ab>0 are used to select the sections. The conversion rules of the coil voltage references into the three-leg voltage references are proposed in Table 2. An example of logic for the conversion rule is given in the Appendix. Here, a and b are the normalized coil voltage references V_1/V_{dc} and V_2/V_{dc}, while V_a, V_b, and V_c are the three-leg voltages.

3.2 Driving an AMB system

The heteropolar radial AMB (Fig. 6) is most widely used in rotating machinery applications. It consists of eight poles and four electromagnets (EM), with the coils of two adjacent poles serially connected. Therefore, two three-leg voltage source converters are required to drive a radial AMB. Usually, the two opposing electromagnets differentially generate one directional force (F_1 or F_2), and the control currents of the opposing electromagnets have a 180° phase difference. In contrast, in case of dominant unbalance forces, the phase difference of two perpendicular forces (F_1 and F_2) is 90° to compensate for the unbalance forces.

There are two possible coil connection architectures for a radial AMB driven by a three-leg voltage source converter: two opposing electromagnets (EM1+EM3 or EM2+EM4) or two adjacent electromagnets (EM1+EM2 or EM3+EM4). Phase plots of 2D voltage space vector modulations for two-coil connection architectures are shown in Fig. 7.

If the two opposing electromagnets are driven, the phases of the dynamic current across the two coils are normally 180° to generate one directional force. Thus, the three-leg voltage source converter is expected to spend the most time in the second and forth quadrants (the solid straight line in Fig. 7). However, the phases of the coil dynamic current across the

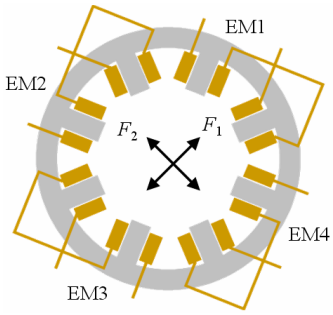

Fig. 6. Heteropolar radial AMB.

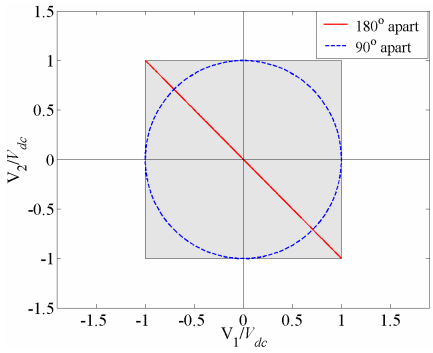

Fig. 7. Voltage space in driving a radial AMB system.

adjacent electromagnets are necessarily 90° apart to produce harmonic forces, and the corresponding coil voltages are 90° phase apart (the dashed circle in Fig. 7). In addition, the available voltage region of the full-bridge scheme with the same DC link voltage is represented by the gray rectangle in Fig. 7. Both the full-performance and the economy driving configurations have smaller voltage regions than the full-bridge configuration, which may lead to the dynamic performance limitation in driving an AMB system.

4. Dynamic performance limitation

4.1 Voltage and current profiles

Simulations of two sinusoidal voltage generations are performed to investigate sinusoidal voltage and current profiles of the 2D space vector modulation for an AMB system. Simulation models of both driving configurations are built, as shown in Fig. 8. The simulation parameters are as follows: the coil has a resistance of 0.6 Ω and inductance of 5.5 mH; and the DC link voltage and the switching frequency are 30 V and 10 kHz, respectively.

In both coil connection architectures, sinusoidal voltages of 30 V amplitude and 10 Hz frequency are generated with each driving configuration. The filtered output PWM voltages are shown in Fig. 9(a). If the full-bridge or the full-performance driving configuration drives the opposing electromagnets, a complete sinusoidal voltage can be produced without any distortion [the dotted curve in Fig. 9(a)]. This is because the voltage region of the full-performance configuration in Fig.

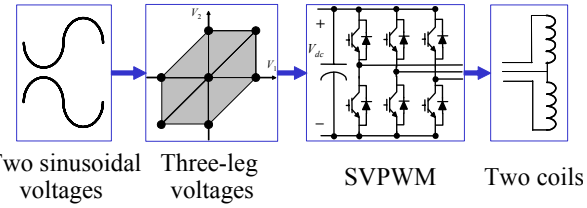

Fig. 8. Block diagram of the simulation model.

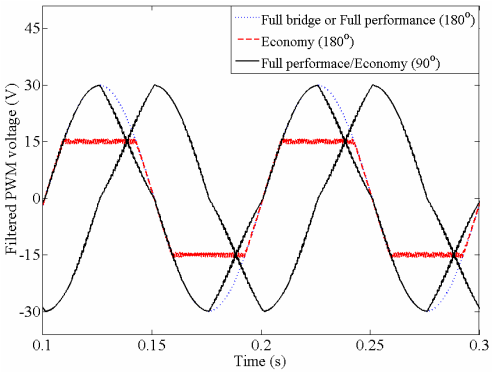

(a) Voltage profiles

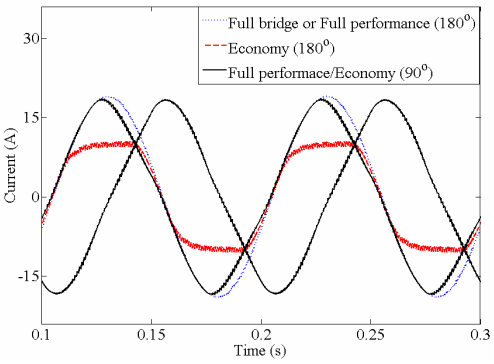

(b) Current profiles

Fig. 9. Voltage and current profiles of the driving configurations.

5(a) completely covers the second and forth quadrants, despite the reduced voltage region in both first and third quadrants. If adjacent electromagnets are driven by the full-performance or the economy driving configuration, a slightly distorted sinusoidal voltage is generated [the solid line in Fig. 9(a)]. In particular, the sinusoidal voltage is distorted because the voltage regions in Fig. 5 cannot cover the voltage region encompassed by the dashed circle in the Fig. 7. In contrast, the economy driving configuration, when applied to the opposing electromagnets, produces a significantly distorted sinusoidal voltage [the dashed curve in Fig. 9(a)]. The corresponding current profiles of the two driving configurations are shown in Fig. 9(b). The corresponding current signals are also distorted by the voltages shown in Fig. 9(a). Specifically, the current of either the full-performance or the economy driving configuration for the adjacent electromagnets has slightly smaller peaks than that of the full-bridge configuration, which leads to a small degradation of the dynamic performance [12, 13].

4.2 Mathematical analysis

Dynamic performance degradations of the driving configurations are mathematically analyzed in this section. The worst case among the driving configurations is the economy configuration for driving the opposing electromagnets. The economy configuration only has half the dynamic performance because it has half the DC link voltage. However, the dynamic performance degradation is not obvious when the adjacent electromagnets are driven by either the full-performance or the economy driving configuration.

A coil of an AMB system can be modeled as a connection of resistance (R) and inductance (L) in series. Currents (i) with a sine wave voltage input of amplitude (V) and frequency (ω) can be obtained through solving the differential equation below:

$$L\frac{di}{dt} + Ri = V\sin\omega t \tag{1}$$

A steady-state solution of the differential equation is

$$i(t) = \frac{V}{L^2\omega^2 + R^2}\left(R\sin\omega t - L\omega\cos\omega t\right) \tag{2}$$

We assume a voltage profile like the solid line in Fig. 9 (a). The voltage profile is a sine wave before $t = \pi/2\omega$, therefore, the current at $t = \pi/2\omega$ should be $VR^2/(L^2\omega^2 + R^2)$ from Eq. (2). The differential equation after $t = \pi/2\omega$ can be expressed by Eq. (3):

$$L\frac{di}{dt} + Ri = \frac{2V\omega}{\pi}\left(\frac{\pi}{\omega} - t\right), i\left(\frac{\pi}{2\omega}\right) = \frac{VR}{L^2\omega^2 + R^2} \tag{3}$$

The solution after applying initial conditions is given by

$$i(t) = -\frac{V}{R}\left(\frac{L^2\omega^2}{L^2\omega^2 + R^2} + \frac{2\omega}{\pi}\frac{L}{R}\right)e^{\frac{R}{L}\left(\frac{\pi}{2\omega} - t\right)} + \frac{V}{R}\frac{2\omega}{\pi}\left(\frac{\pi}{\omega} + \frac{L}{R} - t\right) \tag{4}$$

The current has the peak value when the differentiation of the solution is zero. The time when the derivative of Eq. (4) becomes zero can be expressed by

$$t = \frac{L}{R}\ln\left(1 + \frac{\pi}{2\omega}\frac{R}{L}\frac{L^2\omega^2}{L^2\omega^2 + R^2}\right) + \frac{\pi}{2\omega} \tag{5}$$

The peak current can be calculated by substituting the time into Eq. (4):

$$i_p = \frac{V}{R}\left(1 - \frac{2\omega}{\pi}\frac{L}{R}\ln\left(1 + \frac{\pi}{2\omega}\frac{R}{L}\frac{L^2\omega^2}{L^2\omega^2 + R^2}\right)\right) \tag{6}$$

Normalized peak currents and the relative dynamic performance degradations at various dimensionless frequencies ($\tau = \omega L/R$) are shown in Fig. 10. The peak current is normalized dividing the currents by a factor of V/R. The peak current

Table 3. Comparison of normalized peak currents.

Full bridge	Proposed driving configurations
$\frac{1}{\sqrt{\tau^2+1}}$	$1-\frac{2}{\pi}\tau\ln\left(1+\frac{\pi}{2}\frac{\tau}{\tau^2+1}\right)$

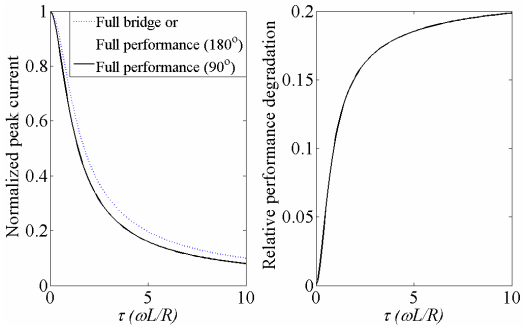

(a) Normalized peak current (b) Performance degradation

Fig. 10. Performance degradation of the driving configurations.

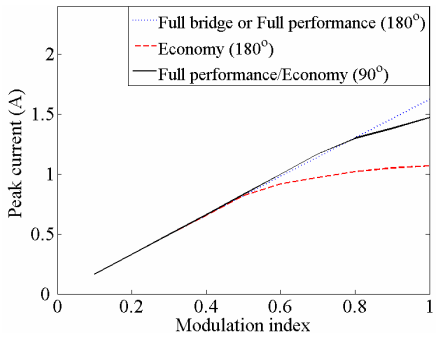

Fig. 11. Peak currents of the proposed driving configurations at various modulation indices (500 Hz).

ratio (the relative performance degradation) increases as the dimensionless frequency increases. The normalized peak currents of two driving configurations are compared in Table 3.

4.3 Simulations

Simulations of the 2D space vector modulation with the proposed driving configurations are performed. The coil parameters are the same in the previous section. A modulation index (generated voltage amplitude over DC link voltage, V_{ref}/V_{DC}) varies from 0.1 to 1 (3 to 30 V), and a normalized frequency (generated voltage frequency over switching frequency) is varied from 0.01 to 0.1 (100 to 1000 Hz).

The peak currents of both driving configurations for two coil connection architectures are calculated at various modulation indices and fixed normalized frequency (0.05) in, as shown in Fig. 11. The peak currents of the two driving configurations (90° apart) appear to be smaller than those of the full-bridge driving configuration when the modulation index is greater than 0.71. Moreover, the economy configuration covers only the half-voltage space of two opposing electromagnets (180° apart), which results in the clamped peak current where the modulation index is over 0.5 (Fig. 11). This is because the available voltage region of both driving configurations in Fig. 5 is smaller than the required voltage space for driving a radial AMB in Fig. 7.

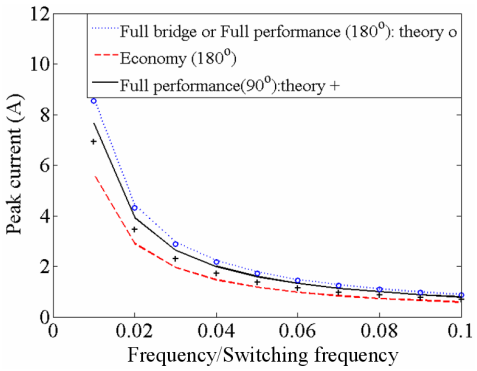

Fig. 12. Peak currents of the proposed driving configurations at various frequencies (30 V).

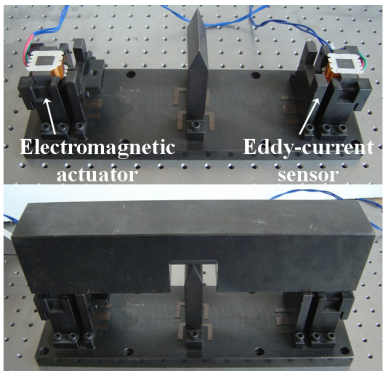

Fig. 13. Single DOF AMB test rig.

The peak currents of both driving configurations for the coil connection architectures of an AMB system are calculated using various normalized frequency and fixed modulation index (1), as shown in Fig. 12. The results of the mathematical analysis agree with the simulation results.

5. Experiments

5.1 Experimental set-up

A constructed single DOF AMB test rig [14] is shown in Fig. 13. The balance of the beam is maintained by electromagnetic actuators on both sides, which are controlled using the measured position of the beam with an eddy-current sensor. The length of the beam is 329 mm, the mass of the beam is 11.31 kg, the nominal air gap of the actuator is 0.35 mm, and the nominal coil inductance and resistance are 5.5 mH and 0.6 Ω, respectively.

A block diagram of the AMB controller is shown in Fig. 14. The controller consists of three main parts: PID position controllers, PI current controllers, and PWM generations. A DSP control system with a 6-channel 12-bit AD and a 14-channel 14-bit PWM is adopted. The DC link voltage is 30 V and the sampling (switching) frequency is 10 kHz.

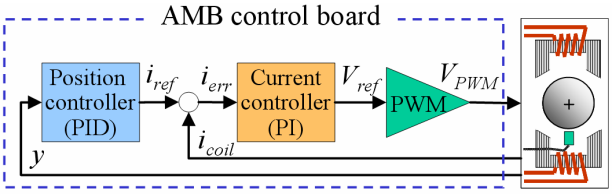

Fig. 14. Block diagram of the controller.

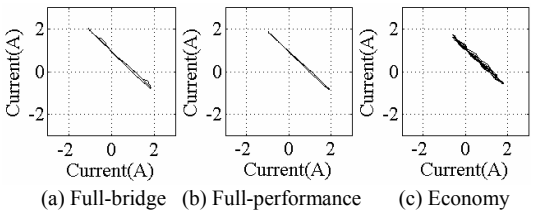

Fig. 15. Phase plot of currents excited by voltage of 180° phase difference (500 Hz and 25 V).

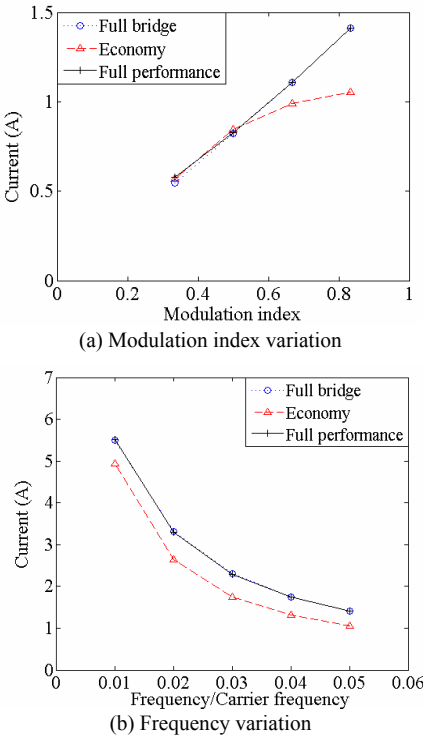

Fig. 16. Currents excited by two harmonic voltages of 180° phase difference.

To verify the simulation results, high-frequency voltage excitation experiments are performed during the levitation of the single DOF AMB system. As two harmonic voltage excitation signals are added to the voltage reference (V_{ref} in Fig. 14) of the current controller, the current and voltage signals of two coils are measured. Both the magnitude and frequency of the voltage excitation signal are from 10 to 25 V and from 100 to 500 Hz, respectively. The voltage excitation signals have a phase difference of either 90° or 180°.

For the current signal to follow the high-frequency voltage excitation signal, the bandwidth of the PI current controller is

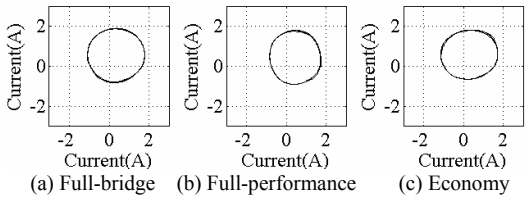

Fig. 17. Phase plot of currents excited by voltages of 90° phase difference (500 Hz and 25 V).

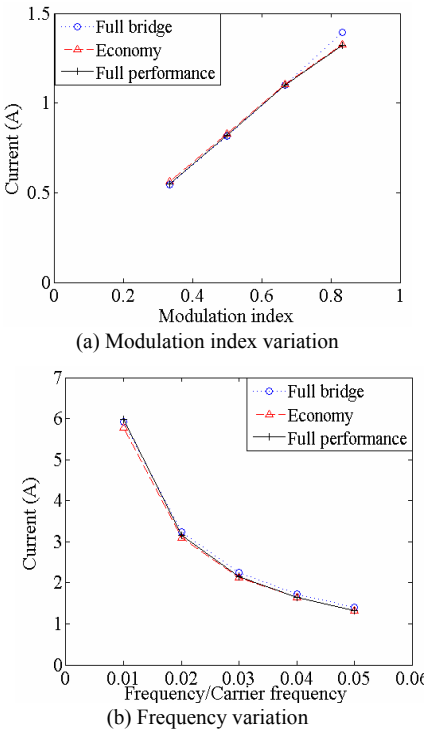

Fig. 18. Currents excited by two harmonic voltages of 90° phase difference.

lowered to 25 Hz, which is five times lower than the voltage excitation signals.

5.2 Experimental results

In the case that two harmonic voltage excitation signals with 25 V (modulation index: 0.833) and 500 Hz (normalized frequency: 0.05) have a phase difference of 180°, the phase plots of two current signals in three driving configurations (i.e., full-bridge, full-performance, and economy) are shown in Fig. 15. The phase plots of two current signals form straight lines of different magnitudes.

Two harmonic voltages with 500 Hz and 180° phase difference are injected. The current magnitudes according to the modulation index of the voltage excitation signals are shown in Fig. 16(a). The current magnitudes according to voltage excitation signals of various normalized frequencies and fixed amplitude (25 V) are shown in Fig. 16(b). The currents of both full-bridge and the full-performance driving configurations have the same magnitudes, whereas those of the economy driving configuration have significantly smaller magnitudes.

In the case that two harmonic voltage excitations with 25 V and 500 Hz have a phase difference of 90°, the phase plots of the current signals are shown in Fig. 17. The phase plots of harmonic voltages with 90° phase difference forms an ideal circle (dashed line in Fig. 7). However, the non-linearity of the AMB system results in a slightly distorted circle of the current phase plot (Fig. 17(a)), which has small offsets in the center due to the bias current. In particular, large distortions of both full-performance and economy configurations (Figs. 17(b) and (c)) are caused by their reduced voltage region (Figs. 5(a) and (b), respectively).

In the case of two harmonic voltage excitations with 500 Hz and a 90° phase difference, current magnitudes (mean value of major and minor axes of current phase plot) according to the voltage excitations of various modulation indices are shown in Fig. 18(a). The currents of both the full-performance and the economy driving configurations have smaller magnitudes than the full-bridge configuration when the modulation index is greater than 0.71. In addition, the current magnitudes of fixed amplitude voltage excitation (25 V) according to normalized frequency are shown in Fig. 18(b). The performance degradation and current of Fig. 18(b) are smaller than those of Fig. 12 because the modulation index is not 1 but 0.833 (25/30).

The experiment results show good agreement with the simulation results and prove that a proper choice of the coil connection architecture can minimize the dynamic performance degradation in driving an AMB system with three-leg voltage source converters.

6. Conclusion

This paper presented methodologies for driving an AMB system using a 2D space vector modulation of three-leg voltage source converters. Two driving configurations were proposed: full-performance and economy. The economy configuration is more cost-effective than the half-bridge driving configuration. The conversion rules for two coil voltage references of an AMB system into three-leg voltage references of the converter were developed. The performance limitations of proposed driving configurations were discussed both analytically and numerically, and were subsequently verified with experiments using a single DOF AMB system.

Acknowledgement

This work was supported by the Korea Institute of Science and Technology (KIST) and by the Ministry of Knowledge Economy (MKE), Korea, under the "program for CITG" support program supervised by the National IT Industry Promotion Agency" (NIPA-C6150-1001-0004).

References

[1] G. Schweitzer, H. Bleuler and A. Traxler, *Active magnetic bearings*, Hochschulverlag AG, ETH Zurich, Switzerland (1994).

[2] H. J. Ahn and D. C. Han, System modeling and robust control of an AMB spindle: Part I Modeling and validation for robust control, *KSME International*, 17 (12) (2003) 1855-1866.

[3] Fairchild semiconductor inc., *Smart power module user's guide*, Application note 9018, Sep. (2001).

[4] J. Holtz, Pulsewidth modulation - A survey, *IEEE Trans. on Industrial Electronics,* 39 (5) (1992) 410-420.

[5] H. W. van der Broeck, H. C. Skudelny and G. Stanke, Analysis and realization of a pulse width modulator base on voltage space vectors, *IEEE Trans. on Industrial Applications*, 24 (1988) 142-150.

[6] J. Zhang., *Power amplifier for active magnetic bearings*, Ph.D. thesis, ETH Zurich, Switzerland (1995).

[7] P. Buhler, R. Siegwart and R. Herzog, Digital Control for Low Cost Industrial AMB Applications, *Proc. 5th ISMB*, Kanazawa, Japan (1996) 83-88.

[8] R. Schob, C. Redemann and T. Gempp, Radial active magnetic bearing for operation with a 3-Phase power converter, *Proc. 4th ISMST*, Gifu, Japan (1997) 111-124.

[9] J. S. Yim, J. H. Kim, S. K. Sul, H. J. Ahn, I. H. Park, D. C. Han and S. H. Choi, A novel cost-effective scheme of power amplifier for AMBs using space vector technology, *Proc. 8th ISMB*, Ibaraki, Japan, Aug. (2002).

[10] H. J. Ahn, Dynamic Performance Limitation in Driving a Radial AMB with Space Vector PWM, *Proc. 11th ISMB*, Nara, Japan, Aug. (2008).

[11] D.-H. Jang and D.-Y. Yoon, Space-vector PWM technique for two phase inverter-fed two-phase induction motors, *IEEE trans. on Industrial Applications*, 39 (2) (2003) 542-549.

[12] E. H. Maslen, P. Hermann, M. A. Scott and R. R. Humphris, Practical limits to the performance of magnetic bearings: peak force, slew rate, and displacement sensitivity, *Journal of Tribology*, 111 (2) (1989) 331-336.

[13] K. R. Bamstein, Dynamic load capabilities of active electromagnetic bearings, *Journal of Tribology*, 113 (3) (1991) 598-603.

[14] J. D. Lindlau and C. R. Knospe, Feedback linearization of an active magnetic bearing with voltage control, *IEEE Trans. on Control Systems Technology*, 10 (1) (2002) 21-31.

Appendix

An example logic to convert two-coil voltage references into three-leg voltage references is described here. Table A1 shows the switching sequence of section 1 of right half-plane in Fig. 5(a). The symmetric PWM is considered and two zero switching states [i.e., (0, 0, 0) and (1, 1, 1)] are placed at two ends of the switching sequence.

If the total switching time is T_s (= T_0 + T_1 + T_2), the switching time of each leg is calculated as follows: the normalized coil voltages of (1, 0) and (0, 1) are applied during T_1 and T_2 in case of section 1 of right half-plane in Fig. 5(a); therefore, T_1 and T_2 should be a T_s and b T_s. The switching times of the

Table A1. Switching sequence of section 1 of right half-plane in Fig. 5(a).

	$T_0/2$	T_1	T_2	$T_0/2$	$T_0/2$	T_2	T_1	$T_0/2$
S_a	0	1	1	1	1	1	1	0
S_b	0	0	1	1	1	1	0	0
S_c	0	0	0	1	1	0	0	0

Table A2. Switching sequence of section 1 of left half-plane in Fig. 5(a).

	$T_0/2$	T_1	T_2	$T_0/2$	$T_0/2$	T_2	T_1	$T_0/2$
S_a	0	0	0	1	1	0	0	0
S_b	0	0	1	1	1	1	0	0
S_c	0	1	1	1	1	1	1	0

three-legs are thus determined as Eq. (A1):

$$S_a \ : \ T_1 + T_2 + \frac{T_0}{2} = \frac{(1+a+b)}{2} T_s \tag{A1a}$$

$$S_b \ : \ T_2 + \frac{T_0}{2} = \frac{(1-a+b)}{2} T_s \tag{A1b}$$

$$S_a \ : \ \frac{T_0}{2} = \frac{(1-a-b)}{2} T_s \tag{A1c}$$

Table A2 shows the switching sequence of section 1 of left half-plane in Fig. 5(a).

Because normalized coil voltages of (0, -1) and (-1, 0) are applied during T_1 and T_2 in case of section 1 of the half-plane in Fig. 5(a), T_1 and T_b should be $-b\ T_s$ and $-a\ T_s$. Therefore, the switching times of the three-legs are determined as Eq. (A2).

$$S_a \ : \ \frac{T_0}{2} = \frac{(1+a+b)}{2} T_s \tag{A2a}$$

$$S_b \ : \ T_2 + \frac{T_0}{2} = \frac{(1-a+b)}{2} T_s \tag{A2b}$$

$$S_a \ : \ T_1 + T_2 + \frac{T_0}{2} = \frac{(1-a-b)}{2} T_s \tag{A2c}$$

Hyeong-Joon Ahn received B.S., M.S. and Ph.D. degrees in School of Mechanical and Aerospace Engineering at Seoul National University in 1995, 1997 and 2001, respectively. He was a Research Associate of the University of Virginia, USA from 2002 to 2003 and worked as a BK21 Assistant Professor at Seoul national University from 2004 to 2005. Prof. Ahn is currently an Assistant Professor at the Department of Mechanical Engineering in Soongsil University. He is also currently serving as an Editor of International Journal of Rotating Machinery. His research interests are in the area of rotordynamics, control, and mechatronics.

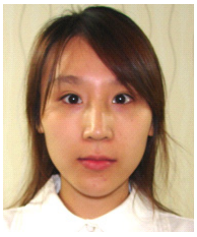

Se-Na Jeong received her B.S. degree in Department of Mechanical En-gineering at Soongsil University in 2009. She is currently a masteral student at Department of Mechanical Engineering in Soongsil University. Her research interests are in the area of magnetic bearing and control.